Controlled deposition of fullerene derivatives within a graphene template by means of a modified Langmuir-Schaefer method

Kouloumpis, Antonios; Vourdas, Nikolaos; Zygouri, Panagiota; Chalmpes, Nikolaos; Potsi, Georgia; Kostas, Vasilios; Spyrou, Konstantinos; Stathopoulos, Vassilis N.; Gournis, Dimitrios; Rudolf, Petra

Published in:
Journal of Colloid and Interface Science

DOI:
10.1016/j.jcis.2018.04.049

Document Version
Publisher's PDF, also known as Version of record

Publication date:
2018

Journal of Colloid and Interface Science 524 (2018) 388–398

Contents lists available at ScienceDirect

Journal of Colloid and Interface Science

journal homepage: www.elsevier.com/locate/jcis

Regular Article

Controlled deposition of fullerene derivatives within a graphene template by means of a modified Langmuir-Schaefer method

Antonios Kouloumpis [a,b,*], Nikolaos Vourdas [c], Panagiota Zygouri [a,b], Nikolaos Chalmpes [a], Georgia Potsi [a,b], Vasilios Kostas [a], Konstantinos Spyrou [a], Vassilis N. Stathopoulos [c], Dimitrios Gournis [a,*], Petra Rudolf [b,*]

[a] Department of Materials Science and Engineering, University of Ioannina, GR-45110 Ioannina, Greece
[b] Zernike Institute for Advanced Materials, University of Groningen, Nijenborgh 4, NL-9747AG Groningen, The Netherlands
[c] School of Technological Applications, Technological Educational Institute of Sterea Ellada, 34400 Psachna, Evia, Greece

GRAPHICAL ABSTRACT

Scheme 2. A bottom-up layer-by-layer approach was applied for the integration of fullerene derivatives into graphene oxide by combining the self-assembly with the Langmuir-Schaefer deposition technique. Graphene oxide nanosheets were used as a template for accommodating C_{60} derivatives ($C_{60}(OH)_{24}$ and $C_{60}Br_{24}$) within the interlayer space.

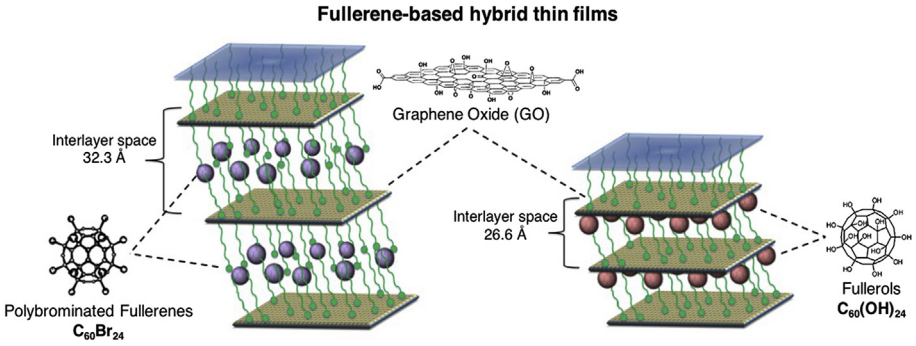

ARTICLE INFO

Article history:
Received 21 December 2017
Revised 23 March 2018
Accepted 10 April 2018
Available online 12 April 2018

Keywords:
Langmuir-Blodgett
Self-assembly
Graphene
Hybrids
Fullerene derivatives
Thin films

ABSTRACT

The scientific and technological potential of graphene's includes the development of light, open 3D hybrid structures with high surface area, tunable pore size and aromatic functionalities. Towards this aim, we describe a scalable and low-cost bottom-up approach that combines self-assembly and Langmuir-Schaefer deposition for the production of fullerene-intercalated graphene oxide hybrids. This method uses graphene oxide (GO) nanosheets as template for the attachment of two types of fullerene derivatives (bromo-fullerenes, $C_{60}Br_{24}$ and fullerols, $C_{60}(OH)_{24}$) in a bi-dimensional arrangement, allowing a layer-by-layer growth with control at nanoscale. Our film preparation approach relies on a bottom-up process that includes the formation of a hybrid organo-graphene Langmuir film, which is transferred onto a substrate and then brought in contact with $C_{60}(OH)_{24}$ molecules in solution to induce self-assembly. In the case of grafting $C_{60}Br_{24}$ molecules into graphene a further modification of the GO platelets was performed by bringing the surface of the transferred GO Langmuir film in contact with a second amino surfactant solution. Repeating these deposition cycles, pillared structures were fabricated in thin films form.

* Corresponding authors at: University of Ioannina, GR-45110 Ioannina, Greece (A. Kouloumpis).
E-mail addresses: antoniokoul@gmail.com (A. Kouloumpis), dgourni@cc.uoi.gr (D. Gournis), p.rudolf@rug.nl (P. Rudolf).

https://doi.org/10.1016/j.jcis.2018.04.049

These fullerene-based hybrid thin films were characterized by Raman and X-ray photoelectron (XPS) spectroscopies, X-ray diffraction (XRD), Atomic Force Microscopy (AFM) and contact angle measurements.

1. Introduction

Buckminster fullerene (C_{60}) was discovered in 1985 by Kroto, Curl and Smalley [1]; it consists of 60 sp^2 carbon atoms arranged in pentagons and hexagons to form a spherical nanostructure (cage) [2]. Due to the size and electronic structure of C_{60} and larger fullerenes, derivatives can be formed by inserting atoms or molecules inside the cage (endohedral fullerenes) and by functionalizing with substituents outside the cage (exohedral fullerenes). As most organic molecular materials, fullerenes and their derivatives can be insulators, semiconductors, or even superconductors when doped with other atoms or molecules [3,4]. These tunable conductivity properties render them very attractive as active materials for electronic devices, such as light detectors, transistors, or solar cells [3,5].

Although halogenated fullerene derivatives are interesting for their outstanding physical and chemical properties, investigations of their potential for diverse applications are still scarce [6–8]. However the presence of halogens in other carbon materials has been studied already decades ago. Doping with bromide was demonstrated to increase the electrical conductivity of graphite [9,10], and carbon nanotubes [11,12]. More specifically, S. Tongay et al. [13] fabricated a superconductive bromine-intercalated graphite by exposing highly ordered pyrolytic graphite (HOPG) to bromine vapor [13]; with the same method Jung N. et al. [14] achieved an enhancement of the conductivity for multilayered graphene films and thick graphite. Bromine derivatives of graphene that could be used for reversible bromine storage or as a starting material for further chemical modifications were synthesized by O. Jankovsky [15] and co-workers in 2014. In the same year, Klouda Karel et al. [8] synthesized hybrid brominated nanostructures containing fullerene molecules within graphene oxide by reacting graphene oxide with brominated fullerene derivatives ($C_{60}Br_{14\text{-}18}$) and by direct bromination (with liquid bromide) of an oxidized GO-C_{60} mixture. These authors reported that the brominated materials thermally decomposed at higher temperatures than the unbrominated ones, due to the retarding action of bromine [8]. A. E. Mansour et al. [16] investigated the doping of graphene with bromine to develop high performance transparent conducting electrodes.

The functionalization of a fullerene cage can also be a first step in the synthesis of more complex derivatives with different physical and chemical properties [3,5]. In this context the halogenation of fullerenes (with fluorine, chlorine, or bromine) is one of the most common chemical reactions to yield derivatives that can be either used as they are or serve as precursors in substitution reactions to sequentially attach aromatic groups to the fullerene cage [17–20]. In the case of brominated fullerene the substitution of the bromine with OH groups results in derivatives with better solubility in water and in aqueous solutions [21,22]. Polyhydroxylated fullerene or fullerols ($C_{60}(OH)_n$), have attracted much scientific and industrial attention in engineering [23–25], where they were found to improve the corrosion resistance and microhardness of coatings [23], to give better mechanical properties than C_{60}, when incorporated in poly(styrene-*co*-4-vinylpyridine), in catalysis [26–28], for optical limiting performance [24] or to reinforce and have antioxidation effects when mixed with natural rubber to inhibit the decrease of tensile strength after aging [25]. Fullerols improve have been proposed for performing bio-oxidations [29,30]. They have been tested as agents for Parkinson's disease (PD) prevention and therapy [31,32], and as active compounds in the preparation of skin rejuvenation cosmetic formulations [33], just to name a few of the many fields of science and technology [34–37] where $C_{60}(OH)_n$ have been considered.

In addition, since fullerols have better solubility in water than brominated fullerene, nanotechnology can tune and control the fundamental physicochemical properties of fullerenes derivatives by ordering them into molecular thin films [38–47] fabricating either hydrophilic or hydrophobic nanocoatings. The possibility to control the size and the orientation of fullerene moieties in 2D arrangements can lead to new functional low-dimensional materials with interesting and promising properties for controllable wetting applications [26] including corrosion resistant [48], smart textiles [49], self-cleaning [50] and directional wetting [51] surfaces as well as for developing lab-on-a-chip (LOC) devices [52] and biosensors [26].

Our recent study in incorporating pure C_{60} within graphene matrices revealed an improvement in the electrical conductivity of hybrid films by fabricating graphene nanobuds [47]. Concerning the need of hybrid thin films and nanocoatings with more complex derivatives and with different or enhanced physical and chemical properties in combination with the need of devising hybrid materials through facile and economic production methods, here we report a bottom-up layer-by-layer approach for the integration of fullerene derivatives into graphene oxide by combining the self-assembly with the Langmuir-Schaefer (LS) deposition technique. Graphene oxide (GO) nanosheets were used as a template for accommodating C_{60} derivatives (fullerol with chemical formula $C_{60}(OH)_{24}$ and bromo-fullerene with chemical formula $C_{60}Br_{24}$) within the interlayer space. More specifically, a dilute water suspension of chemically oxidized graphene was used as subphase in a Langmuir-Blodgett trough and an amino surfactant, which covalently binds to GO, was applied for the formation of hybridized GO platelets in the air-suspension interface. After the transfer of the hybrid GO Langmuir film using the Langmuir-Schaefer method (horizontal dipping), the substrate was dipped into a solution of fullerols ($C_{60}(OH)_{24}$ to induce self-assembly (SA). Instead, in the case of grafting $C_{60}Br_{24}$, after the transfer of the hybrid GO Langmuir film using the Langmuir-Schaefer method (horizontal dipping), the substrate was first brought in contact with another amino surfactant solution to induce functionalization by self-assembly and then, as the final step, lowered in the solution of the bromo-fullerene to complete the self-assembly with the $C_{60}Br_{24}$ molecules. Hybrid graphene oxide multilayer thin films hosting fullerene-derivatives molecules within their interlayer space were fabricated by repeating these two procedures, as illustrated in Scheme 1. The samples were characterized by Raman and X-ray photoelectron spectroscopies, X-ray diffraction, Atomic Force Microscopy and contact angle measurements.

2. Experimental section

2.1. Materials

Buckminster fullerene (99.8%), octadecylamine (ODA, ≥99%), hexamethylenediamine (HEX, ≥99%) acetone, methanol and ethanol were purchased from Sigma-Aldrich. Sodium hydroxide (NaOH) pellets were obtained from Vioryl. Ultrapure deionized water (18.2 MOhm) produced by a Millipore Simplicity® system

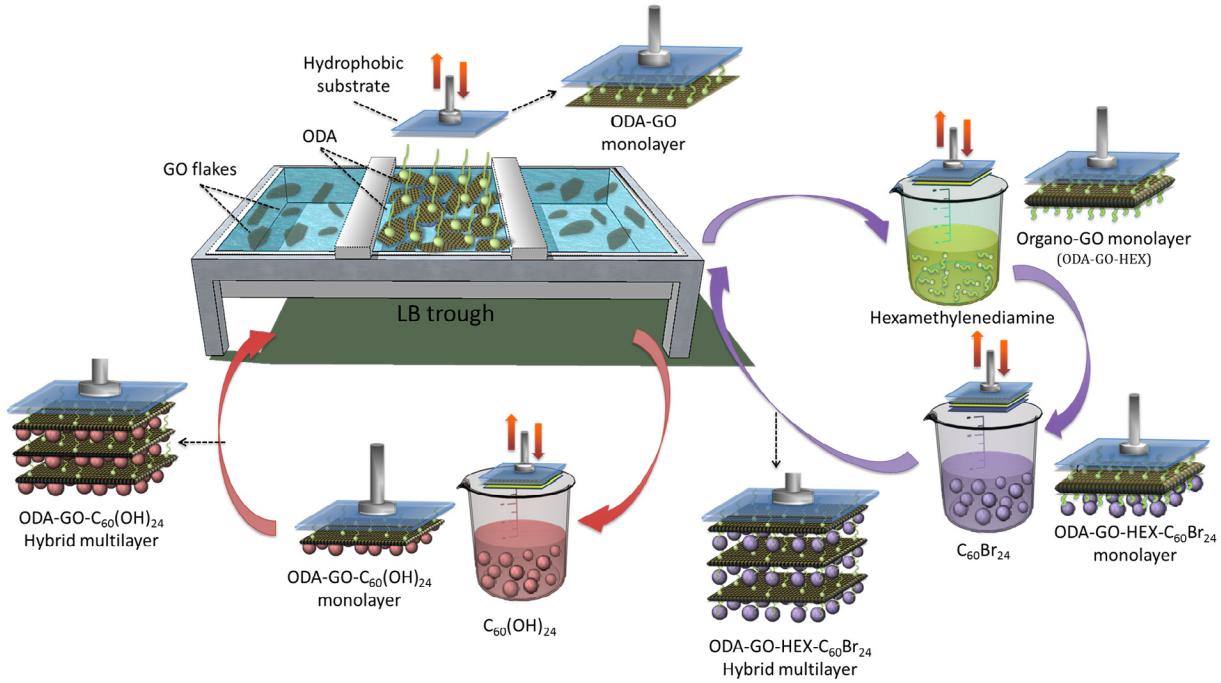

Scheme 1. Schematic representation of the synthetic procedures followed for fabricating hybrid films of (left) graphene oxide and $C_{60}(OH)_{24}$ (ODA-GO-$C_{60}(OH)_{24}$) and (right) graphene oxide and $C_{60}Br_{24}$ (ODA-GO-HEX-$C_{60}Br_{24}$). Both procedures consist in a Langmuir-Schaefer deposition combined either with one self-assembly step (left) or two self-assembly steps (right).

was used throughout. The Si wafers (P/Bor, single side polished, purchased from Si-Mat) used as substrates were cleaned prior to use by ultrasonication in water, acetone, and ethanol for 15 min each. All reagents were of analytical grade and were used without further purification.

2.2. Synthesis of graphene oxide

Graphene oxide was produced from graphite using a modified Staudenmaier method [53–56]. In a typical synthesis, 10 g of powdered graphite (purum, powder $\leq$ 0.2 mm; Fluka) were added to a mixture of 400 mL of 95–97% H_2SO_4 and 200 mL of 65% HNO_3, while cooling in an ice-water bath. 200 g of powdered $KClO_3$ were added to the mixture in small portions under vigorous stirring and cooling in an ice-water bath. The reaction was quenched after 18 h by pouring the mixture into ultrapure water and the oxidation product was washed until the pH reached 6.0. Finally, the sample was dried at room temperature.

2.3. Synthesis of fullerene derivatives

Fullerene derivatives were synthesized as described in detail elsewhere [22]. In a typical synthesis of polybrominated fullerene ($C_{60}Br_{24}$), 300 mg of Buckminster fullerene were dissolved in 2 mL of elementary bromine, in the presence of a catalytic quantity of $FeBr_3$. The mixture was stirred for 40 min at room temperature. When the reaction was completed, the excess of unreacted bromine was evaporated and the catalyst was separated by dissolving in a mixture of ethanol/H_2O (1:2, v/v). Polyhydroxylated fullerene (fullerol, $C_{60}(OH)_{24}$) was synthesized by using polybrominated fullerenes as precursor [22]. More specifically, fullerol was obtained by reacting 50 mg of $C_{60}Br_{24}$ with 5 mL of NaOH aqueous solution 2 M (pH = 13) for 2 h at room temperature. After completion of the reaction, the solvent was evaporated at 40 °C; then the mixture was filtered and washed 5 times with 10 mL of ethanol (purity 70%). The dark brown powder product obtained after the filtration was soluble in polar solvents like water [22].

2.4. Preparation of hybrid multilayers of graphene oxide and C_{60}-derivatives

A Langmuir Blodgett (LB) trough (KSV 2000 Nima Technology) was cleaned with ethanol and distilled-deionized water. GO suspensions in ultrapure water (0.02 mg mL^{-1}) were prepared and used as subphase. To achieve the hybridization of the GO sheets in the LB trough, 200 μL of a 0.2 mg mL^{-1} ODA dissolved in a chloroform/methanol mixture (9/1, v/v) were spread onto the water surface using a microsyringe. After a waiting time of 20 min to allow for solvent evaporation and functionalization of ODA to occur at the top side of GO surface, the hybrid ODA-GO layer was compressed at a rate of 5 mm min^{-1} until the chosen stabilization pressure of 20 mN m^{-1} was reached. This pressure was maintained throughout the deposition process. The hybrid Langmuir layers (ODA-GO) were transferred onto the Si-wafer substrates by horizontal dipping (Langmuir Schaefer technique), with downward and lifting speeds of 10 and 5 mm min^{-1}, respectively [47,57]. After the horizontal lift of a substrate, the ODA-GO film was dipped into an aqueous solution of fullerols (0.2 mg mL^{-1}). A hybrid graphene/$C_{60}(OH)_{24}$ multilayer film was constructed by repeating this procedure for 60 times, as shown in Scheme 1 (sample denoted as ODA-GO-$C_{60}(OH)_{24}$). For the formation of the hybrid graphene oxide film hosting polybrominated fullerene in its interlayer space, a further surface modification of the GO nanosheets was performed by bringing the surface of the transferred Langmuir film (ODA-GO) in contact with a amino surfactant, HEX dissolved in methanol (0.2 mg mL^{-1}), and making use of a self-assembly step [47,54]. After this functionalization, in a final stage, the hybrid organo-GO (ODA-GO-HEX) film was lowered into a solution of polybrominated fullerene (0.2 mg mL^{-1}) dissolved in a ethanol/H_2O mixture (2/1, v/v) to induce the formation of a hybrid ODA-GO-HEX-$C_{60}Br_{24}$ layer by self-assembly. By repeating this procedure 60 times, a hybrid multilayer film was constructed as shown in Scheme 1 (sample denoted as ODA-GO-HEX-$C_{60}Br_{24}$) where the surface termination of each hybrid film contains a fullerene-derivative plane layer. Moreover, every time when the substrate was lowered, it was

allowed to touch the air-water interface or the solution surface in a very gentle dip of max 0.5 mm below the liquid surface for 90s. After each deposition step samples were rinsed several times by dipping into ultrapure water (to eliminate any weakly attached cations or molecules that remained from the deposition steps) and dried with nitrogen flow (to avoid contaminating either the LB air-water interface or the other solutions) [44,58].

3. Characterization techniques

Atomic force microscopy (AFM) images of single layers of ODA-GO and ODA-GO-$C_{60}(OH)_{24}$ or ODA-GO-HEX-$C_{60}Br_{24}$ deposited on Si wafers were collected in tapping mode with a Bruker Multimode 3D Nanoscope, equipped with a microfabricated silicon cantilever type TAP-300G, with a tip radius <10 nm and a force constant of ~ 20–75 N m^{-1}. Raman spectra were recorded with a Micro-Raman system RM 1000 RENISHAW using a laser excitation line at 532 nm. A 0.5–1 mW laser power was used with a 1 μm focus spot in order to avoid photodecomposition of the hybrid multilayers. Powder samples of C_{60} and $C_{60}Br_{24}$ were measured using a Labram Horiba HR spectrometer integrated with a laser line at 514 nm. A 1.5 mW laser power was used with a 2 μm focus spot. X-ray photoelectron spectroscopy (XPS) data of the hybrid multilayers were collected at a base pressure of $5 * 10^{-10}$ mbar in a SPECS GmbH spectrometer equipped with a monochromatic Mg Kα source (hv = 1253.6 eV) and a Phoibos-100 hemispherical analyzer. The energy resolution was set to 1.16 eV and the photoelectron take-off angle was 37° with respect to the surface normal. All binding energies were referenced to the C1s core level photoemission line at 284.6 eV. Spectral analysis included a Shirley background subtraction and a peak deconvolution employing mixed Gaussian-Lorentzian functions, in a least squares curve-fitting program (WinSpec) developed at the Laboratoire Interdisciplinaire de Spectroscopie Electronique, University of Namur, Belgium. X-ray diffraction (XRD) patterns of the hybrid multilayers were collected on a D8 Advance Bruker diffractometer by using Cu Kα (40 kV, 40 mA) radiation and a secondary beam graphite monochromator. The patterns were recorded in the 2-theta (2θ) range from 1.5 to 15°, in steps of 0.02° and with a counting time of 2 s per step. Infrared spectra covering the spectral range 400–4000 cm^{-1} were measured with a Shimadzu FT-IR 8400 infrared spectrometer, equipped with a deuterated triglycine sulphate (DTGS) detector. Each spectrum was the average of 128 scans collected at 2 cm^{-1} resolution. Fullerene derivatives were in the form of KBr pellets containing *ca.* 2 wt% of $C_{60}(OH)_{24}$ or $C_{60}Br_{24}$. Thermogravimetric (TGA) and differential thermal (DTA) analyses were performed using a Perkin Elmer Pyris Diamond TG/DTA. Powder samples of approximately 5 mg were heated in air from 25 °C to 850 °C, at a rate of 5 °C/min. Water contact angle (CA) measurements were performed by a SL200 KS contact angle meter from Kino at ambient atmospheric conditions. 5 μL distilled water droplets were used for all CA measurements. The CAs were recorded from the time the droplet touched the surface (CA t = 0) until CA reached a plateau value, approximately 1 min after the first touch (CA t = 1 min). After this first static mea-

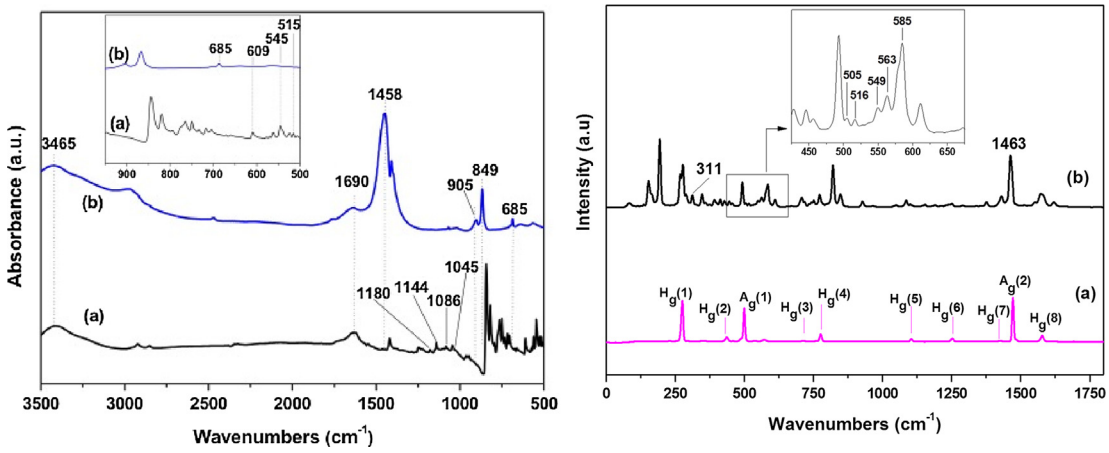

Fig. 1. Left: FTIR spectra of (a) polybrominated fullerene ($C_{60}Br_{24}$) and (b) fullerol ($C_{60}(OH)_{24}$). **Right:** Raman spectra of (a) Pristine Buckminster fullerene and (b) polybrominated fullerene ($C_{60}Br_{24}$).

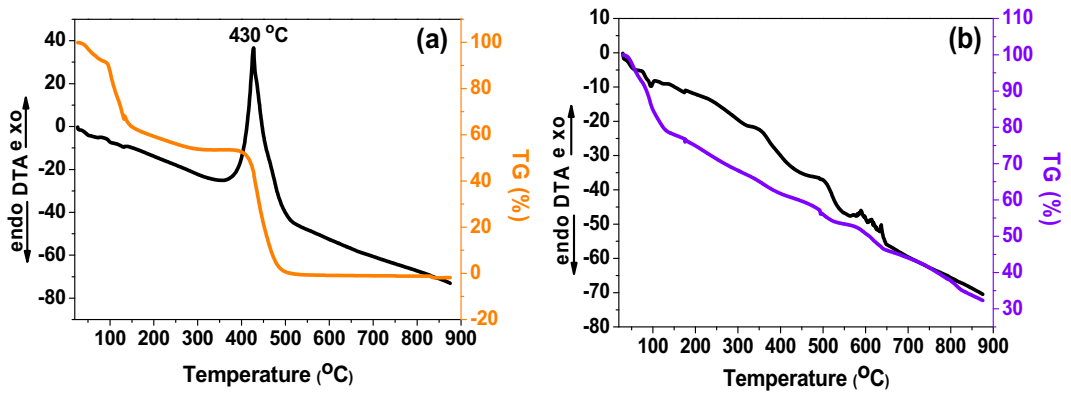

Fig. 2. Thermogravimetric analysis (TGA) and thermal analysis (DTA) measurements of (a) polybrominated ($C_{60}Br_{24}$) and (b) polyhydroxylated fullerenes ($C_{60}(OH)_{24}$).

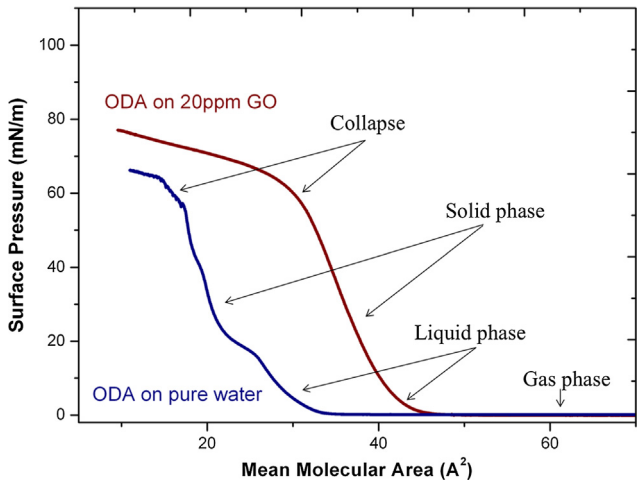

Fig. 3. π-A isotherms recorded during the compression of ODA monolayers both on pure water and on an aqueous suspension of 20 mg dm^{-3} GO.

surement and at the same point, dynamic water CA measurements were performed. Advancing and receding CA were measured on a water droplet of decreasing/increasing volume [59].

4. Results-discussion

4.1. Structural characterization of C_{60} derivatives

FTIR spectra of polybrominated fullerene ($C_{60}Br_{24}$) and fullerol ($C_{60}(OH)_{24}$) are shown in Fig. 1 (left). In the case of polybrominated fullerene, the stretching vibrations of the C-Br groups were observed in the range of 500–610 cm^{-1} (515 cm^{-1}, 545 cm^{-1} and 609 cm^{-1}) [60]. Based on the Sadtler Handbook of Infrared spectra [61] bands in the region of 1000–1200 cm^{-1} can be attributed to vibrations of C-Br groups; for $C_{60}Br_{24}$, these bands appear at 1045 cm^{-1}, 1086 cm^{-1}, 1144 cm^{-1}, 1180 cm^{-1}. The FTIR spectrum of $C_{60}(OH)_{24}$ is typical for fullerols shows characteristic bands due to the presence of hydroxyl groups at 1065 and 1458 cm^{-1} (bending vibrations of C-OH groups), as well as at 685 cm^{-1}, 849 cm^{-1} and 905 cm^{-1} (wagging vibrations of OH). The bands at 3465

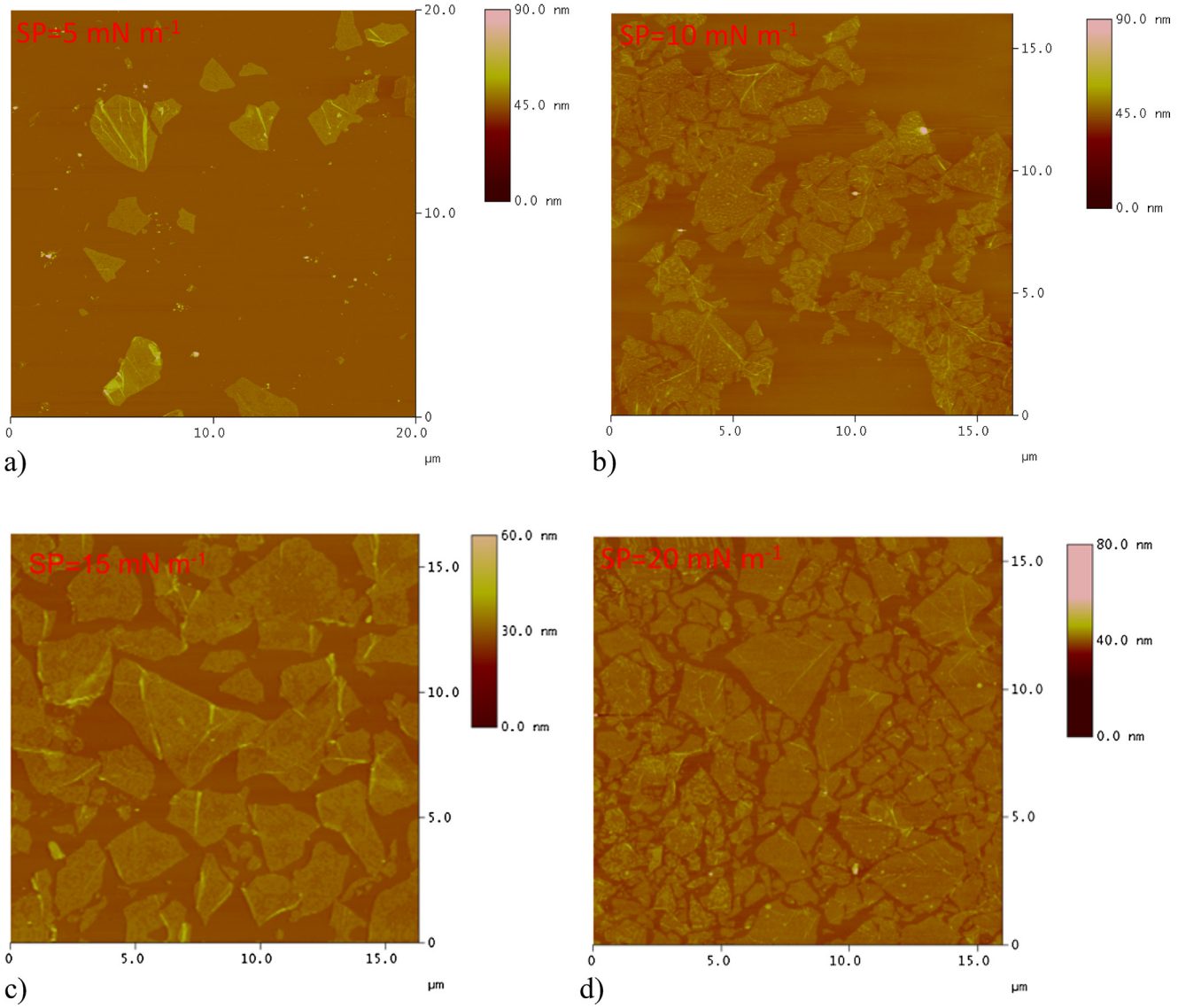

Fig. 4. AFM height images of ODA-GO monolayers deposited on Si-wafer substrates at different surface pressures of (a) 5 mN m^{-1}, (b) 10 mN m^{-1}, (c) 15 mN m^{-1} and (d) 20 mN m^{-1} during the compression process.

cm^{-1} (stretching vibration) and 1690 cm^{-1} (bending vibration) are instead indicative of the presence of water molecules. The band at 3465 cm^{-1} corresponds to the stretching vibration of the —OH bond and is observed also in liquid water. These data are in agreement with similar FTIR features of fullerols as described elsewhere [22].

Raman spectra of pristine and polybrominated fullerene ($C_{60}Br_{24}$) are shown in Fig. 1 (right). C_{60} is characterized by high I_h symmetry and presents 46 vibrational modes distributed over the 174 vibrational degrees of freedom. From the 46 vibrational modes, 4(T_{1u}) are active in the infrared region and 10 ($2A_g + 8H_g$) are active in Raman, while the remaining are optically inactive [62].

$$\Gamma_{vib}(C_{60}) = 2A_g(\text{Raman}) + 3F_{1g} + F_{2g} + 6G_g + 8H_g(\text{Raman}) + A_u + 4F_{1u}(\text{IR}) + 5F_{2u} + 6G_u + 7H_u$$

In the case of polybrominated fullerene, the bromines are attached to the twelve six-membered rings of the fullerene structure at the 1 and 4 position induce a "boat" conformation, while for the remaining 8 six-membered rings, the bromine atoms bound to the carbons 1, 3 and 5, create a "chair" conformation [63,64]. The active vibrations of the C-Br groups are five, more specifically stretching vibrations of these groups are observed at 505 cm^{-1}, 516 cm^{-1}, 549 cm^{-1}, 562 cm^{-1} and 585 cm^{-1}. The presence of the band at 1463 cm^{-1} in the spectra of the $C_{60}Br_{24}$, corresponds to the Ag symmetry of the fullerene, indicating that the icosahedral structure remains unaffected after the functionalization. The appearance of a new band at 308 cm^{-1} can be attributed to a neutral molecular Br_2 in a charge transfer complex between C_{60} and Br_2 [65,66].

Thermogravimetric analysis (TGA) and thermal analysis (DTA) measurements for polybrominated and polyhydroxylated fullerene are presented in Fig. 2**.** The TGA curve of $C_{60}Br_{24}$ (a) presents a 9% weight loss up to 100 °C corresponding to absorbed water and unreacted molecular bromine (Br_2). At the temperature range between 100 and 180 °C, a mass loss (~31%) is observed, which can be attributed to the removal of functional groups. The curve of DTA shows an exothermic peak at 430 °C related to the combustion of the fullerene carbon cage, which is followed by the total weight loss of the sample (~60 wt%). In the case of fullerols (b), a mass loss of ~20 wt% in the temperature range up to 120 °C, points to the presence of naturally absorbed water molecules and demonstrates the hydrophilic character of the $C_{60}(OH)_{24}$. The removal of the hydroxyl groups occurs between 150 and 320 °C, and corresponds to a weight loss of ~13%. Above 350 °C the decomposition of the carbon structure resulting in a weight loss close to 37%. The removal of the hydroxyl groups and the decomposition of the fullerene are not separated in the DTA curve, indicating an interdependence of these two phenomena, and consequently testifying to the successful chemical functionalization of the fullerene.

4.2. Structural control of hybrid monolayers

To demonstrate the attachment of octadecylamine (ODA) surfactant to the graphene oxide (GO) flakes, we recorded (π-A) isotherms of the surface pressure versus the mean molecular area while compressing the Langmuir film by means of the movable barriers of the LB trough. Fig. 3 displays the π-A isotherms of an ODA monolayer both on pure water and on a GO suspension. The curves show changes in slope corresponding to the phase transi-

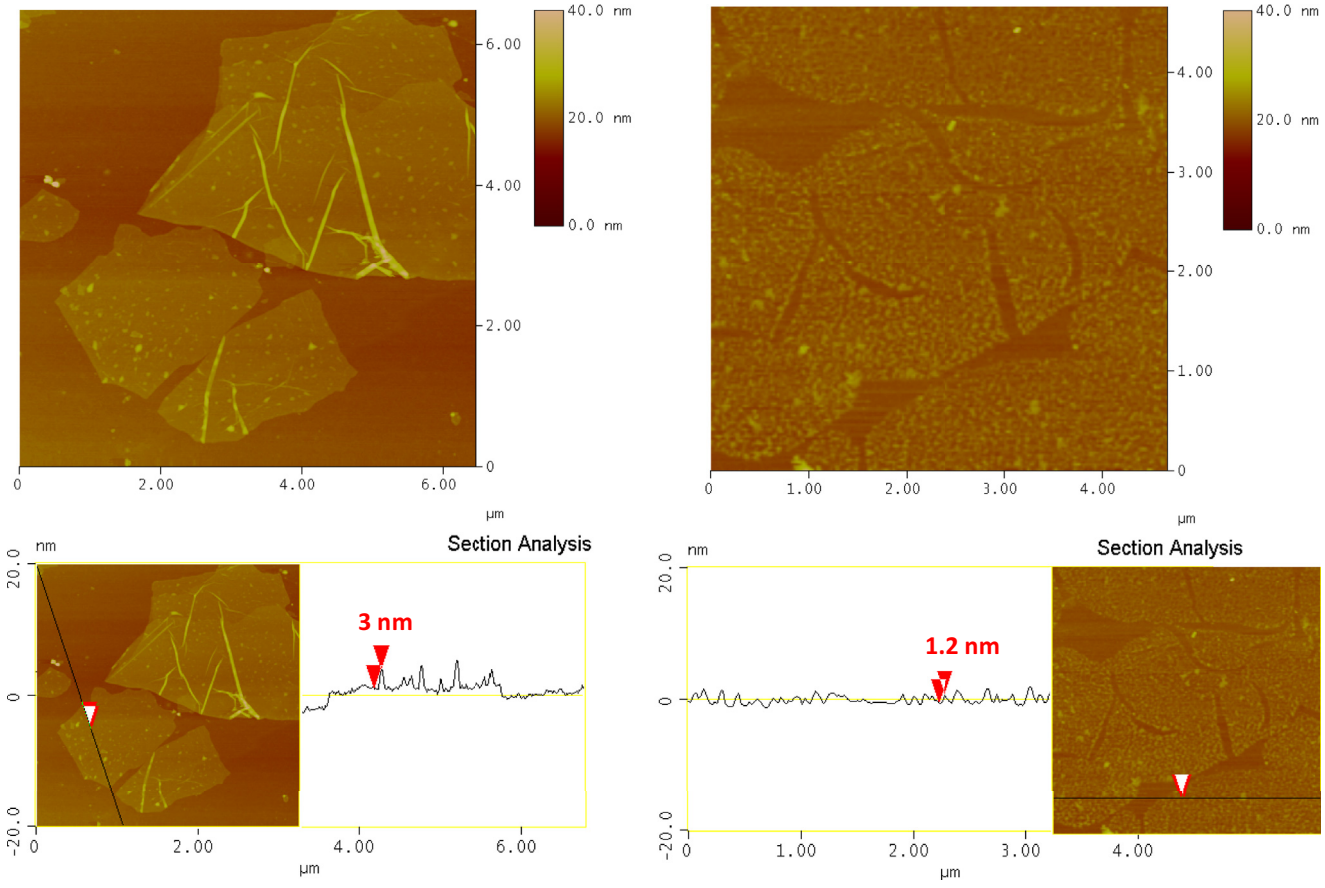

Fig. 5. AFM height images and cross section analysis profile of ODA-GO-HEX-$C_{60}Br_{24}$ (left) and ODA-GO-$C_{60}(OH)_{24}$ (right) hybrid single layers.

tions from two dimensional gas to condensed liquid and then to solid during the compression process. The fact that the compression of ODA on top of the GO suspension gives rise to an increase the surface pressure much earlier during the compression compared to that for ODA spread on pure water, indicates that a hybrid floating layer of functionalised ODA-GO has been formed [47,57], that is related to the hybridization of GO nanosheets by covalent bonding via the amide functionality of ODA [67].

Representative AFM images of hybrid Langmuir monolayers (ODA-GO) transferred onto the Si-wafer at different surface pressures in the LB trough, namely 5, 10, 15 and 20 mN/m, are shown in Fig. 4**.** The topographic images revealed that the substrate surface coverage of the hybrid ODA-GO monolayers is higher as the surface pressure increases. GO nanosheets with well-defined edges are easily observed in the AFM micrographs, verifying the formation of a hybrid Langmuir film at the air-suspension interface. More specifically, when the Langmuir film was compressed at 5 mN m^{-1} (Fig. 4a), the GO platelets appear isolated with an empty space between them. When the Langmuir film was further compressed at 10 mN m^{-1} (Fig. 4b), the GO platelets contact each other, with still rather large voids between them and at even higher surface pressure of 15 mN m^{-1} (Fig. 4c), the nanosheets become more closely packed. When deposited at 20 mN m^{-1} the hybrid film becomes very dense but with only very few overlaps between adjacent flakes (Fig. 4d). Furthermore, the GO layers exhibit an amplitude of wrinkles that may be related to water-GO interactions during the dipping and drying process. GO sheets can be wrinkled during water evaporation due to surface tension [68,69]. The average thickness of the flakes is 1–1.5 ± 0.2 nm as derived from topographical height profile (section analysis) corresponding to the size of single graphene oxide layers.

Detailed AFM images of single ODA-GO-HEX-$C_{60}Br_{24}$ and ODA-GO-$C_{60}(OH)_{24}$ hybrid layers deposited on Si-wafer are shown in Fig. 5. The micrographs reveal the presence of quite uniform and nearly spherical particles decorating several micrometer size layers indicating the successful attachment of the C_{60} derivatives on the graphene oxide surface while wrinkled sheets were also observed. More specifically, the $C_{60}Br_{24}$ decoration in the hybrid ODA-GO-HEX monolayer is relatively uniform revealing small particles in all over the surface of the GO sheets. In the other hand, the hybrid ODA-GO-$C_{60}(OH)_{24}$ layer exhibit a smoother distribution and higher coverage of $C_{60}(OH)_{24}$ molecules on the graphene oxide layers as compared to $C_{60}Br_{24}$ in the hybrid ODA-GO-HEX-$C_{60}Br_{24}$ layer. This different morphology is due to the direct attachment of $C_{60}(OH)_{24}$ to the polar oxygen-containing groups homogeneously distributed on the graphitic surface (without interposed surfactant like in the case of brominated fullerene). The average size of decorating $C_{60}Br_{24}$ and $C_{60}(OH)_{24}$ molecules was about 3 ± 0.2 nm and 1.8 ± 0.2 nm respectively as deduced from the height profile analysis. The larger size of the $C_{60}Br_{24}$ moieties arises probably from the presence of the hexamethylenediamine (HEX) molecules attached between the $C_{60}Br_{24}$ and GO nanosheets during the 2nd self-assembly step of the synthetic approach.

4.3. Characterization of graphene/C_{60}-derivative hybrid multilayers

The X-ray diffraction patterns of the produced ODA-GO-HEX-$C_{60}Br_{24}$ and ODA-GO-$C_{60}(OH)_{24}$ hybrid multilayers (60 layers) are shown in Fig. 6 (top). The hybrid multilayer with $C_{60}Br_{24}$ shows a 001 diffraction peak at $2\theta = 2.3°$ from which a d_{001}-spacing of 38.4 Å is deduced. This d_{001} value corresponds to an interlayer space of $\Delta = 38.4–6.1 = 32.3$ Å, where the value of 6.1 Å represents the thickness of the GO single layer [70], indicating the successful insertion of the $C_{60}Br_{24}$ molecules as pillars between GO sheets. Moreover, the presence of higher order (0 0 l) reflections in the XRD pattern of ODA-GO-HEX-$C_{60}Br_{24}$ suggests very high order in

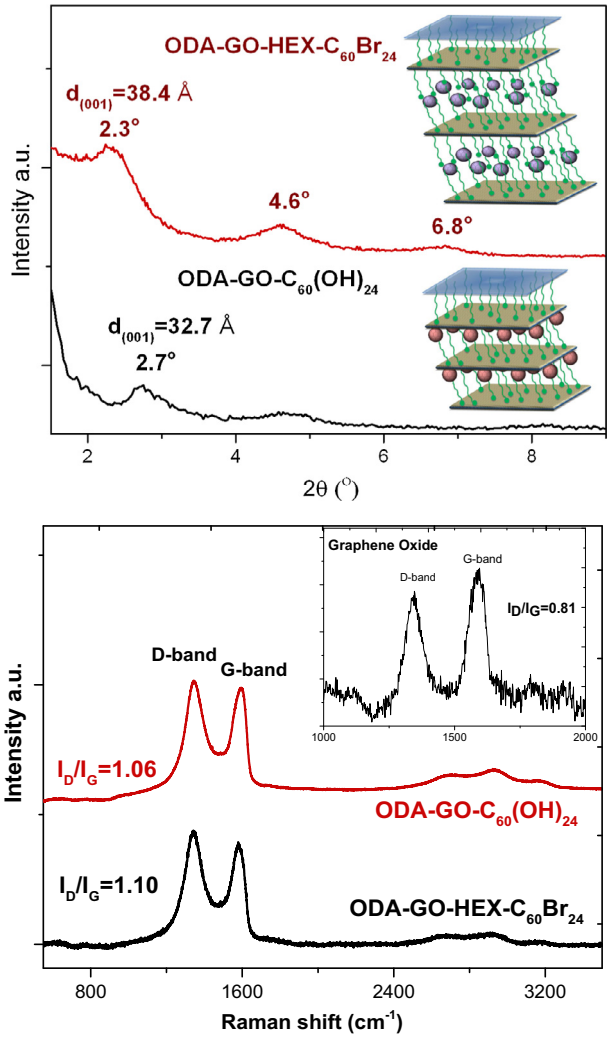

Fig. 6. Top: XRD patterns and schematic illustration (inset) of ODA-GO-HEX-$C_{60}Br_{24}$ and ODA-GO-$C_{60}(OH)_{24}$ hybrid multilayers (60 layers). **Bottom:** Raman spectra of ODA-GO-HEX-$C_{60}Br_{24}$ and ODA-GO-$C_{60}(OH)_{24}$ hybrid multilayers (inset: Raman spectrum of graphene oxide).

the stacking of the GO layers. On the other hand, the ODA-GO-$C_{60}(OH)_{24}$ hybrid multilayer shows a 0 0 1 diffraction peak at $2\theta = 2.7°$, resulting in a smaller d_{001}-spacing of 32.7 Å. This value corresponds to an interlayer space of $\Delta = 32.7–6.1 = 26.6$ Å, testifying to the presence of $C_{60}(OH)_{24}$ molecules in the interlayer space [71]. This value is smaller as compared to the d_{001}-spacing of ODA-GO-HEX-$C_{60}Br_{24}$ because the $C_{60}(OH)_{24}$ molecules are directly attached to the graphene oxide layers without an interposed surfactant. Since the nucleus diameter of fullerenes and fullerene derivatives is less than 10 Å [72–74] while the size of ODA and HEX molecules is 23 Å and 4.5 Å respectively, we conclude that both surfactants must adopt a configuration with the linear alkyl chains to be inclined within the interlayer space of graphene oxide layers.

The Raman spectra of the produced ODA-GO-HEX-$C_{60}Br_{24}$ and ODA-GO-$C_{60}(OH)_{24}$ hybrid multilayers deposited on a Si wafer are shown in Fig. 6 (bottom). Spectra of graphene-based thin films exhibit the characteristics bands. The second order D band at around 1350 that is connected to sp^3 hybridized carbon arising from lattice defects and distortions while the first order G band at around 1600 cm^{-1} is linked with sp^2 hybridized carbon atoms of the graphitic lattice [75,76]. The ratio of the D- to G-band intensities (I_D/I_G) is indicative of the quality of the graphitic lattice and was found to be 0.81 for the pristine GO (Fig. 6 bottom, inset)

which is in agreement with typical GO I_D/I_G values found in the literature [77,78]. The ratio of the D- to G-band intensities (I_D/I_G) for the hybrids ODA-GO-HEX-$C_{60}Br_{24}$ and ODA-GO-$C_{60}(OH)_{24}$ multilayers is 1.1 and 1.06 respectively. This increase of the I_D/I_G ratio in the case of the hybrid films could be assigned to the relative increase of the bands related to the graphitic disorder (D band at 1350 cm^{-1} and D' band at 1620 cm^{-1}) suggesting the hybridization of GO due to the covalent bonding of the amide functionalities [79] of ODA and HEX. Moreover, both spectra displays three broad bands in the 2D region at ~2700, ~2930 and ~3200 cm^{-1} which are typical of GO materials. These are related with the 2D (or else G') vibrational mode, the D + D' mode, and the 2D' mode in that order [75,76,80].

In order to gain further information for the type of bonding between the graphite oxide layers and the C_{60} derivatives we employed x-ray photoelectron spectroscopy measurements. Fig. 7 (top) displays C1s and N1s core level region of the ODA-GO-$C_{60}(OH)_{24}$ hybrid multilayer. Four contributions located at binding energies of 284.6 eV, 286.1 eV, 287.2 eV and 288.6 eV can be identified. The peak at 284.6, which accounts for 61.1% of the total carbon intensity, originates from the carbon-carbon bonds of graphite oxide and of the fullerene cage, as well the C—C of ODA. The peak at 286.1 eV is due to C—O of GO and of the hydroxyl groups of fullerol. The same peak also contains contributions from C—N bonds of ODA molecules when reacted with the epoxy groups of graphite oxide. The contribution at 287.2 eV is due to C═O (carbonyl) as well C—O—C (epoxy) functional groups and accounts for 10.7% of the total carbon intensity. A last peak centered at 288.6 eV stems from carboxyl groups of graphite oxide (3.1%). Additionally there is no observation of the characteristics shake up peaks of C_{60} [81] due to the delocalization of the pi electrons from the anchoring hydroxyl groups of fullerol [82,83]. In the Nitrogen 1s photoelectron spectra we identify three contributions, one at 399.3 eV attributed to C—N—C bond of ODA with the epoxy groups of graphite oxide, a second one at 400.8 eV corresponding to the primary amines that may interact with the GO surface by non-covalent bonding, and a third one, which originates from the protonated amines of ODA-GO-$C_{60}(OH)_{24}$.

Fig. 7 (bottom) shows the C1s and N1s photoelectron spectra of the ODA-GO-HEX-$C_{60}Br_{24}$ hybrid multilayer. The main contribu-

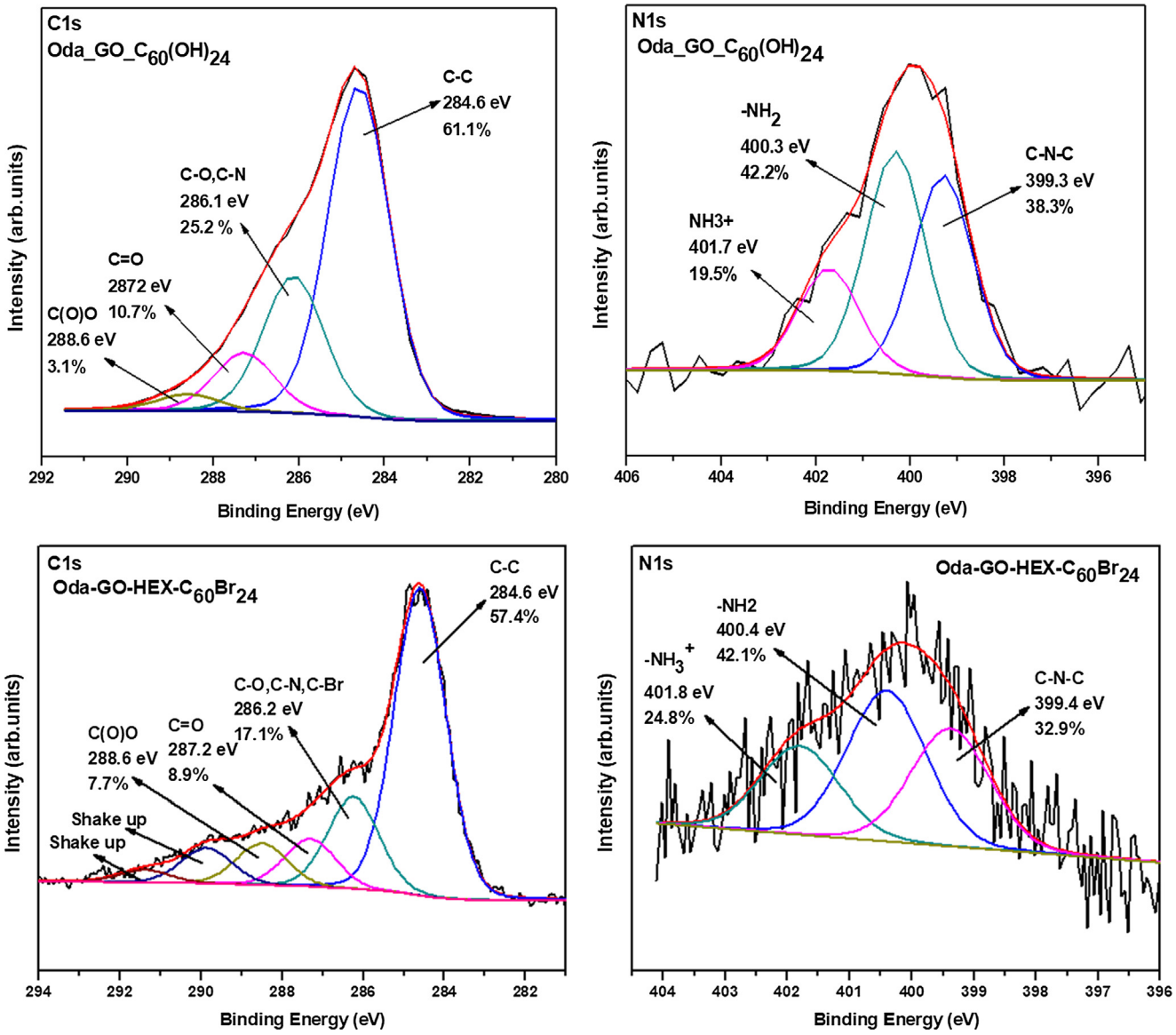

Fig. 7. Top: C1s (left) and N1s (right) core level X-ray photoemission spectrum of a ODA-GO-$C_{60}(OH)_{24}$ hybrid multilayer film. **Bottom:** C1s (left) and N1s (right) core level X-ray photoemission spectrum of the ODA-GO-HEX-$C_{60}Br_{24}$ hybrid multilayer film.

Table 1
Water contact angle measurements.

Sample	CA (t = 0)	CA (t = 1 min)	Advancing CA	Receding CA
ODA-GO-HEX-$C_{60}Br_{24}$ (30 layers)	59 ± 1°	55 ± 1°	64 ± 1°	<20 ± 1°
ODA-GO-$C_{60}(OH)_{24}$ (30 layers)	98 ± 1°	85 ± 1°	103 ± 1°	40 ± 1°

tion to the C1s line at 284.6 eV binding energy results from carbon-carbon bonds of graphite oxide and of the fullerene cage, as well as from the C—C bonds of ODA and accounts for 57.4% of the total carbon intensity. A less intense peak (17.1%) arises from the C—O of GO and the C—Br bond of fullerene derivative and contains also contributions from C—N bonds of ODA molecules due to the chemical grafting of the amino groups of ODA with the epoxy groups of GO. The contribution at 287.2 eV is attributed to the C═O (carbonyl) as well C—O—C (epoxy) functional groups and accounts for 8.9% of the total carbon intensity while the presence of carboxyl groups is demonstrated from the peak located at 288.6 eV (7.7%). The additional peaks at 290.0 eV and 291.5 eV in the ODA-GO-HEX-$C_{60}Br_{24}$ spectrum are due to C1s shake up features of C_{60} [84,85] resulting from π–π^* transitions excited in the photoemission process, and therefore gives proof to the presence of fullerene derivatives in the hybrid multilayer. From the Nitrogen 1s photoelectron spectra of hybrid ODA-GO-HEX-$C_{60}Br_{24}$ multilayer we identify three contributions like in the case of ODA-GO-$C_{60}(OH)_{24}$, one at 399.4 eV attributed to C—N—C bond of ODA and/or HEX molecules with the epoxy groups of graphite oxide, a second one at 400.8 eV corresponding to the primary amines that may interact with the GO surface by non-covalent bonding or lie down on the graphene surface unreacted, and a third one, which derives from the protonated amines of ODA-GO-HEX-$C_{60}Br_{24}$ system. Furthermore, we observe an increase of the NH_3^+ amines of the hybrid ODA-GO-HEX-$C_{60}Br_{24}$ multilayer implying that a higher percentage of NH_3^+ amines interact electrostatically with the graphene surface resulting a lower C—N—C peak (32.9% of the total N1s intensity) compared to the C—N—C peak (38.3% of the total N1s intensity) of the hybrid ODA-GO-$C_{60}(OH)_{24}$ film.

Water contact angle (CA) measurements are presented in Table 1. The CA for the ODA-GO-$C_{60}(OH)_{24}$ hybrid multilayer film results systematically higher than that of the ODA-GO-$C_{60}Br_{24}$ hybrid multilayer film, with the first exhibiting CA = 85° and the latter CA = 55°, ca. 1 min after the droplet touches the surfaces. Both advancing and receding CA are higher for the ODA-GO-$C_{60}(OH)_{24}$ system.

Despite the fact that $C_{60}(OH)_{24}$ molecules are considered to be more hydrophilic than of $C_{60}Br_{24}$ due to the —OH functionalities, our results from CA measurements revealed that the hybrid ODA-GO-$C_{60}(OH)_{24}$ system exhibits a more hydrophobic character compared to the more hydrophilic character of the ODA-GO-HEX-$C_{60}Br_{24}$ system. AFM studies revealed a more uniform distribution of the $C_{60}(OH)_{24}$ molecules on the graphene layer compared to the ODA-GO-HEX-$C_{60}Br_{24}$ system. However, the hydrophilic behaviour of the ODA-GO-HEX-$C_{60}Br_{24}$ film, compared to the more hydrophobic behaviour of the ODA-GO-$C_{60}(OH)_{24}$ is corroborated by the XPS data provided above. As mentioned previously the absence of C_{60} shake up peaks indicates anchoring of hydroxyl groups of fullerol. Moreover as may be seen in Fig. 7, the contributions of the hydrophilic C(O)O (7.7% of the total C1s intensity) and NH_3^+ (24.8% of the total N1s intensity) groups for ODA-GO-HEX-$C_{60}Br_{24}$, are greater than the corresponding ones for ODA-GO-$C_{60}(OH)_{24}$ (3.1% of the total C1s intensity and 19.5% of the total N1s intensity), while the contribution due to aliphatic/hydrophobic carbon bonds (C—C) is higher for ODA-GO-$C_{60}(OH)_{24}$ (61.1% of the total C1s intensity) than for ODA-GO-HEX-$C_{60}Br_{24}$ (57.4% of the total C1s intensity).

5. Conclusions

$C_{60}(OH)_{24}$ and $C_{60}Br_{24}$ fullerene derivatives molecules were effectively inserted between graphene oxide layers through a layer-by-layer synthetic approach, which combines Langmuir-Schaefer deposition and self-assembly steps. The effectiveness of this method in terms of uniformity, coverage and single-layer level control of the formed nanostructures was confirmed by π-A isotherms and AFM measurements. X-ray diffraction measurements revealed the successful insertion of $C_{60}Br_{24}$ and $C_{60}(OH)_{24}$ molecules between graphene oxide nanosheets resulting in hybrid multilayer structures. The existence of $C_{60}(OH)_{24}$ and $C_{60}Br_{24}$ in the hybrid system was revealed by X-ray photoelectron spectroscopy, while Raman spectroscopy showed that the insertion of the fullerene derivatives between the graphene oxide nanosheets caused an increase of the I_D/I_G ratio confirming the hybridization of GO due to the covalent bonding of the amide functionality of ODA. Contact angle measurements corroborated the XPS results, revealed the hybrid graphene/$C_{60}(OH)_{24}$ film exhibiting a more hydrophobic character, while graphene/$C_{60}Br_{24}$ hybrid film was more hydrophilic suggesting that the hydrophobicity doesn't depend on the functional groups of the nanomaterials but on the formed morphology of the hybrid systems.

These novel fullerene-based hybrid films are excellent candidate nanomaterials for potential application where graphene is already been studied such us gas/liquid separation [57], sensors [55,58], photovoltaics [86] or electronic devices [54]. Moreover, the different surface properties of the hybrid films are crucial for a plethora of bio-applications since the adsorption or the adhesion of cells or enzymes depends on the surface energy related to the wetting nature of the surface [87,88]. Thus, thin films with different wetting properties could be used as biosensors, diagnostic (lab-on-a-chip) devices as well as smart surfaces for directional wetting, anti-fogging, inkjet printing and thin-film lubrication [89,90].

In conclusion, the synthesis of hybrid films, combining the properties of 2D materials with fullerene derivatives is a great challenge for fabricating novel pillared structures with modified, adjusted or improved properties. The rise of two-dimensional nanomaterials in combination with the tunable conductivity properties of C_{60} moieties can lead to innovative hybrid materials with fascinating (opto)electronic and biomedical properties.

Acknowledgements

This work was supported in part by the "Graphene based electronics" research program of the Stichting voor Fundamenteel Onderzoek der Materie (FOM), part of the Nederlandse Organisatie voor Wetenschappelijk Onderzoek (NWO). A. K. acknowledges the Ubbo Emmius Program for a PhD fellowship.

References

[1] H.W. Kroto, J.R. Heath, S.C. O'Brien, R.F. Curl, R.E. Smalley, C60, Buckminsterfullerene, Nature 318 (6042) (1985) 162–163.
[2] W.I.F. David, R.M. Ibberson, J.C. Matthewman, K. Prassides, T.J.S. Dennis, J.P. Hare, H.W. Kroto, R. Taylor, D.R.M. Walton, Crystal structure and bonding of ordered C60, Nature 353 (6340) (1991) 147–149.
[3] V. Georgakilas, J.A. Perman, J. Tucek, R. Zboril, Broad family of carbon nanoallotropes; classification, chemistry, and applications of fullerenes,

carbon dots, nanotubes, graphene, nanodiamonds, and combined superstructures, Chem. Rev. 115 (11) (2015) 4744–4822.
[4] M.S. Dresselhaus, G. Dresselhaus, P.C. Eklund, Chapter 15 - Superconductivity, in: Science of Fullerenes and Carbon Nanotubes, Academic Press, San Diego, 1996, pp. 616–653.
[5] P. Scharff, Fundamental properties and applications of fullerene and carbon nanotube systems, in: Frontiers of Multifunctional Nanosystems, Springer Netherlands, Dordrecht, 2002, pp. 213–224.
[6] M. Zachariah, M. Romanini, P. Zygouri, D. Gournis, J.L. Tamarit, M. Barrio, R. Macovez, Variable-range electron hopping, conductivity cross-over and space-charge relaxation in C60br6, Synth. Met. 217 (2016) 123–128.
[7] I. Saikia, A.J. Borah, P. Phukan, Use of bromine and bromo-organic compounds in organic synthesis, Chem. Rev. 116 (12) (2016) 6837–7042.
[8] K. Klouda, E. Zemanova, R. Friedrichova, M. Weisheitova, Fullerene C60, graphene-oxide and graphene-oxide foil with fullerene and their bromination, Int. J. Mater. Sci. Appl. 3 (6) (2014) 293–302.
[9] G. Hennig, The properties of the interstitial compounds of graphite. Iii. The electrical properties of the halogen compounds of graphite, J. Chem. Phys. 20 (9) (1952) 1443–1447.
[10] S. Tadashi, T. Yoichi, M. Takashi, Electrical conductivity of graphite bromine lamellar compounds, Bull. Chem. Soc. Jpn. 43 (1) (1970) 34–38.
[11] R.S. Lee, H.J. Kim, J.E. Fischer, A. Thess, R.E. Smalley, Conductivity enhancement in single-walled carbon nanotube bundles doped with K and Br, Nature 388 (6639) (1997) 255–257.
[12] L.G. Bulusheva, A.V. Okotrub, E. Flahaut, I.P. Asanov, P.N. Gevko, V.O. Koroteev, Y.V. Fedoseeva, A. Yaya, C.P. Ewels, Bromination of double-walled carbon nanotubes, Chem. Mater. 24 (14) (2012) 2708–2715.
[13] S. Tongay, J. Hwang, D.B. Tanner, H.K. Pal, D. Maslov, A.F. Hebard, Supermetallic conductivity in bromine-intercalated graphite, Phys. Rev. B 81 (11) (2010) 115428.
[14] N. Jung, N. Kim, S. Jockusch, N.J. Turro, P. Kim, L. Brus, Charge transfer chemical doping of few layer graphenes, charge distribution and band gap formation, Nano Lett. 9 (12) (2009) 4133–4137.
[15] O. Jankovsky, P. Simek, K. Klimova, D. Sedmidubsky, S. Matejkova, M. Pumera, Z. Sofer, Towards graphene bromide, bromination of graphite oxide, Nanoscale 6 (11) (2014) 6065–6074.
[16] A.E. Mansour, S. Dey, A. Amassian, M.H. Tanielian, Bromination of graphene, a new route to making high performance transparent conducting electrodes with low optical losses, ACS Appl. Mater. Interfaces 7 (32) (2015) 17692–17699.
[17] A. Djordjević, M. Vojínović-Miloradov, N. Petranović, A. Devečerski, D. Lazar, B. Ribar, Catalytic preparation and characterization of C60br24, Fullerene Sci. Technol. 6 (4) (1998) 689–694.
[18] R. Seshadri, A. Govindaraj, R. Nagarajan, T. Pradeep, C.N.R. Rao, Addition of amines and halogens to fullerenes C60 and C70, Tetrahedron Lett. 33 (15) (1992) 2069–2070.
[19] Y. Miyamoto, A. Oshiyama, S. Saito, Halogen doping in solid C60, Solid State Commun. 82 (6) (1992) 437–441.
[20] H. Sekine, H. Maeda, M. Kosuge, Y. Tanaka, M. Tokumoto, Magnetic behavior and structure of the halogen-doped fullerene C60, J. Appl. Phys. 72 (11) (1992) 5448–5450.
[21] A. Djordjevic, B. Srdjenovic, M. Seke, D. Petrovic, R. Injac, J. Mrdjanovic, Review of synthesis and antioxidant potential of fullerenol nanoparticles, J. Nanomater. 2015 (2015) 15.
[22] R. Macovez, E. Mitsari, M. Zachariah, M. Romanini, P. Zygouri, D. Gournis, J.L. Tamarit, Ultraslow dynamics of water in organic molecular solids, J. Phys. Chem. C 118 (9) (2014) 4941–4950.
[23] I.V. Antihovich, N.M. Ablazhey, A.A. Chernik, I.M. Zharsky, Electrodeposition of nickel and composite nickel-fullerenol coatings from low-temperature sulphate-chloride-isobutyrate electrolyte, Procedia Chem. 10 (2014) 373–377.
[24] J. Ouyang, S. Hong Goh, H. Izaac Elim, G. Chen Meng, W. Ji, Dynamic mechanical behavior and optical limiting property of multifunctional fullerenol/polymer composite, Chem. Phys. Lett. 366 (3–4) (2002) 224–230.
[25] H. Kondo, Y. Ohtake, Reinforcement and anti-oxidation effects of natural rubber by fullerol in wet-process method, NIPPON GOMU KYOKAISHI 82 (3) (2009) 98–104.
[26] K. Bhavsar, D. Ross, R. Prabhu, P. Pollard, Led-controlled tuning of Zno nanowires' wettability for biosensing applications, Nano Rev. 6 (1) (2015) 26711.
[27] G. Zhang, Y. Liu, D. Liang, L. Gan, Y. Li, Facile synthesis of isomerically pure fullerenols and formation of spherical aggregates from C60(Oh)8, Angew. Chem. Int. Ed. 49 (31) (2010) 5293–5295.
[28] J. Zhuo, T. Wang, G. Zhang, L. Liu, L. Gan, M. Li, Salts of C60(Oh)8 electrodeposited onto a glassy carbon electrode, surprising catalytic performance in the hydrogen evolution reaction, Angew. Chem. Int. Ed. 52 (41) (2013) 10867–10870.
[29] B. Vileno, P.R. Marcoux, M. Lekka, A. Sienkiewicz, T. Fehér, L. Forró, Spectroscopic and photophysical properties of a highly derivatized C60 fullerol, Adv. Funct. Mater. 16 (1) (2006) 120–128.
[30] R. Injac, M. Prijatelj, B. Strukelj, Fullerenol nanoparticles, toxicity and antioxidant activity, in: D. Armstrong, J.D. Bharali (Eds.), Oxidative Stress and Nanotechnology, Methods and Protocols, Humana Press, Totowa, NJ, 2013, pp. 75–100.
[31] X. Cai, H. Jia, Z. Liu, B. Hou, C. Luo, Z. Feng, W. Li, J. Liu, Polyhydroxylated fullerene derivative C60(Oh)24 prevents mitochondrial dysfunction and oxidative damage in an Mpp+-induced cellular model of Parkinson's disease, J. Neurosci. Res. 86 (16) (2008) 3622–3634.
[32] A. Zhou, J. Zhang, Q. Xie, S. Yao, Application of double-impedance system and cyclic voltammetry to study the adsorption of fullerols (C60(Oh)N) on biological peptide-adsorbed gold electrode, Biomaterials 22 (18) (2001) 2515–2524.
[33] L. Marko, Use of fullerenes in cosmetics, Recent Pat. Biotechnol. 3 (2) (2009) 118–123.
[34] D.G. Letenko, V.A. Nikitin, K.N. Semenov, N.A. Charykov, A.S. Ivanov, Conductivity of aqueous solutions of fullerol synthesized by direct oxidation, Russ. J. Phys. Chem. A 86 (12) (2012) 1808–1815.
[35] D.A. Navarro, R.S. Kookana, M.J. McLaughlin, J.K. Kirby, Fullerol as a potential pathway for mineralization of fullerene nanoparticles in biosolid-amended soils, Environ. Sci. Technol. Lett. 3 (1) (2016) 7–12.
[36] P.A. Indeglia, A. Georgieva, V.B. Krishna, J.-C.J. Bonzongo, Physicochemical characterization of fullerenol and fullerenol synthesis by-products prepared in alkaline media, J. Nanopart. Res. 16 (9) (2014) 1–15.
[37] M. Tomić, A. Vasić-Milovanović, L. Matija, Đ. Koruga, Remanent magnetization measurements of polymeric materials containing fullerol C60(Oh)24 before and after exposure to external magnetic field, Fullerenes, Nanotubes, Carbon Nanostruct. 24 (7) (2016) 423–426.
[38] J.N. Tisserant, P.A. Reissner, S. Jenatsch, H. Beyer, R. Hany, A. Stemmer, Interfacial self-assembly of nanoporous C<Inf>60</Inf> thin films, RSC Adv. 6 (28) (2016) 23141–23147.
[39] V. Santhosh, R. Voggu, P. Chaturbedy, R. Ganapathy, C.N.R. Rao, Mechanical properties of C<Inf>60</Inf> thin films at the air-water interface, Carbon 96 (2016) 1–5.
[40] Y.Q. Zhang, W.J. Wang, S.H. Li, X.X. Gao, B.Y. Zhang, Y.L. Liu, Q.G. Wang, Q. Shi, Langmuir-Blodgett films of a new Diels-Alder adduct of C60 with 1,1'-Biindene, Mater. Sci. Forum (2015) 809–810.
[41] N.K. Minar, K. Hou, C. Westermeier, M. Döblinger, J. Schuster, F.C. Hanusch, B. Nickel, G.A. Ozin, T. Bein, A highly-ordered 3d covalent fullerene framework, Angew. Chem. – Int. Ed. 54 (26) (2015) 7577–7581.
[42] D. Leman, M.A. Kelly, S. Ness, S. Engmann, A. Herzing, C. Snyder, H.W. Ro, R.J. Kline, D.M. DeLongchamp, L.J. Richter, In situ characterization of polymer-fullerene bilayer stability, Macromolecules 48 (2) (2015) 383–392.
[43] H. Kojima, R. Abe, M. Ito, Y. Tomatsu, F. Fujiwara, R. Matsubara, N. Yoshimoto, M. Nakamura, Giant seebeck effect in pure fullerene thin films, Appl. Phys. Express 8 (12) (2015).
[44] R.Y.N. Gengler, D. Gournis, A.H. Aimon, L.M. Toma, P. Rudolf, The molecularly controlled synthesis of ordered bi-dimensional C60 arrays, Chem.-A Eur. J. 18 (24) (2012) 7594–7600.
[45] S.S. Gayathri, A. Patnaik, Interfacial behaviour of brominated fullerene (C60br24) and stearic acid mixed langmuir films at air, Äìwater interface, Chem. Phys. Lett. 433 (4, Äì6) (2007) 317–322.
[46] S. Conoci, D.M. Guldi, S. Nardis, R. Paolesse, K. Kordatos, M. Prato, G. Ricciardi, M.G.H. Vicente, I. Zilbermann, L. Valli, Langmuir-shafer transfer of fullerenes and porphyrins, formation, deposition, and application of versatile films, Chem.-A Eur. J. 10 (24) (2004) 6523–6530.
[47] A. Kouloumpis, K. Dimos, K. Spyrou, V. Georgakilas, P. Rudolf, D. Gournis, A bottom-up approach for the synthesis of highly ordered fullerene-intercalated graphene hybrids, Frontiers Mater. 2 (10) (2015).
[48] T. Xiang, S. Ding, C. Li, S. Zheng, W. Hu, J. Wang, P. Liu, Effect of current density on wettability and corrosion resistance of superhydrophobic nickel coating deposited on low carbon steel Supplement C, Mater. Des. 114 (2017) 65–72.
[49] K.Y. Suh, S. Jon, Control over wettability of polyethylene glycol surfaces using capillary lithography, Langmuir 21 (15) (2005) 6836–6841.
[50] J.H. Chang, I.W. Hunter, Characterization and control of the wettability of conducting polymer thin films, MRS Proc. (2011) 1228.
[51] E. Yu, S.-C. Kim, H.J. Lee, K.H. Oh, M.-W. Moon, Extreme wettability of nanostructured glass fabricated by non-lithographic, Anisotropic Etching 5 (2015) 9362.
[52] Q. Meng, Y. Zhang, J. Li, R.G.H. Lammertink, H. Chen, P.A. Tsai, Altering Emulsion Stability with Heterogeneous Surface Wettability 6 (2016) 26953.
[53] N. Liaros, J. Tucek, K. Dimos, A. Bakandritsos, K.S. Andrikopoulos, D. Gournis, R. Zboril, S. Couris, The effect of the degree of oxidation on broadband nonlinear absorption and ferromagnetic ordering in graphene oxide, Nanoscale 8 (5) (2016) 2908–2917.
[54] R.Y.N. Gengler, A. Veligura, A. Enotiadis, E.K. Diamanti, D. Gournis, C. Jozsa, B.J. van Wees, P. Rudolf, Large-yield preparation of high-electronic-quatity graphene by a Langmuir-Schaefer approach, Small 6 (1) (2010) 35–39.
[55] D.V. Stergiou, E.K. Diamanti, D. Gournis, M.I. Prodromidis, Comparative study of different types of graphenes as electrocatalysts for ascorbic acid, Electrochem. Commun. 12 (10) (2010) 1307–1309.
[56] L. Staudenmaier, Verfahren Zur Darstellung Der Graphitsaure, Ber. Deut. Chem. Ges. 31 (1898) 1481.
[57] A. Kouloumpis, E. Thomou, N. Chalmpes, K. Dimos, K. Spyrou, A.B. Bourlinos, I. Koutselas, D. Gournis, P. Rudolf, Graphene/carbon dot hybrid thin films prepared by a modified langmuir-schaefer method, ACS Omega 2 (5) (2017) 2090–2099.
[58] A. Michopoulos, A. Kouloumpis, D. Gournis, M.I. Prodromidis, Performance of layer-by-layer deposited low dimensional building blocks of graphene-prussian blue onto graphite screen-printed electrodes as sensors for hydrogen peroxide, Electrochim. Acta 146 (2014) 477–484.

[59] N. Vourdas, G. Pashos, G. Kokkoris, A.G. Boudouvis, V.N. Stathopoulos, Droplet mobility manipulation on porous media using backpressure, Langmuir 32 (21) (2016) 5250–5258.
[60] P.R. Birkett, H.W. Kroto, R. Taylor, D.R.M. Walton, R. Ian Grose, P.J. Hendra, P.W. Fowler, The Raman spectra of C60br6 C60br8 and C60br24, Chem. Phys. Lett. 205 (4) (1993) 399–404.
[61] W.W. Simons, The Sadtler handbook of infrared spectra, Sadtler (1978).
[62] H. Kuzmany, R. Pfeiffer, M. Hulman, C. Kramberger, Raman spectroscopy of fullerenes and fullerene-nanotube composites, Philos. Trans. R. Soc. A-Math. Phys. Eng. Sci. 2004 (362) (1824) 2375–2406.
[63] J. Echeverria, D. Casanova, M. Llunell, P. Alemany, S. Alvarez, Molecules and crystals with both icosahedral and cubic symmetry, Chem. Commun. 24 (2008) 2717–2725.
[64] B.W. Clare, D.L. Kepert, Stereochemical patterns in bromofullerenes, C60br12 to C60br24, J. Mol. Struct., THEOCHEM 358 (1) (1995) 79–94.
[65] P.V. Huong, Raman spectra and structure of iodine and bromine intercalated fullerenes C60 and C70, Solid State Commun. 88 (1) (1993) 23–26.
[66] F.N. Tebbe, R.L. Harlow, D.B. Chase, D.L. Thorn, G.C. Campbell, J.C. Calabrese, N. Herron, R.J. Young, E. Wasserman, Synthesis and single-crystal X-ray structure of a highly symmetrical C-60 derivative, C60br24, Science 256 (5058) (1992) 822–825.
[67] A.B. Bourlinos, D. Gournis, D. Petridis, Tamás Szabó, A. Szeri, I. Dekany, Graphite oxide, chemical reduction to graphite and surface modification with primary aliphatic amines and amino acids, Langmuir 19 (15) (2003) 6050–6055.
[68] X. Shen, X. Lin, N. Yousefi, J. Jia, J.-K. Kim, Wrinkling in graphene sheets and graphene oxide papers, Carbon 66 (2014) 84–92.
[69] Y. Chen, F. Guo, A. Jachak, S.-P. Kim, D. Datta, J. Liu, I. Kulaots, C. Vaslet, H.D. Jang, J. Huang, A. Kane, V.B. Shenoy, R.H. Hurt, Aerosol synthesis of cargo-filled graphene nanosacks, Nano Lett. 12 (4) (2012) 1996–2002.
[70] I. Dekany, R. Kruger-Grasser, A. Weiss, Selective liquid sorption properties of hydrophobized graphite oxide nanostructures, Colloid Polym. Sci. 276 (7) (1998) 570–576.
[71] D. Gournis, V. Georgakilas, M.A. Karakassides, T. Bakas, K. Kordatos, M. Prato, M. Fanti, F. Zerbetto, Incorporation of fullerene derivatives into smectite clays, a new family of organic-inorganic nanocomposites, J. Am. Chem. Soc. 126 (27) (2004) 8561–8568.
[72] F.N. Tebbe, R.L. Harlow, D.B. Chase, D.L. Thorn, G.C. Campbell, J.C. Calabrese, N. Herron, R.J. Young, E. Wasserman, Synthesis and single-crystal X-ray structure of a highly symmetrical C≪Sub≫60≪/Sub≫ derivative, C≪Sub≫60≪/Sub≫Br≪Sub≫24≪/Sub&Gt, Science 256 (5058) (1992) 822.
[73] K.N. Semenov, N.A. Charykov, V.N. Postnov, V.V. Sharoyko, I.V. Vorotyntsev, M. M. Galagudza, I.V. Murin, Fullerenols, physicochemical properties and applications, Prog. Solid State Chem. 44 (2) (2016) 59–74.
[74] P.A. Troshin, E. Kemnitz, S.I. Troyanov, Characterization of reactions of fullerene C60 with bromine. Crystal structures of bromofullerenes C60br6, C60br6·Cs2, C60br8·Chbr3·2br2, and C60br24· C6h4cl2·Br 2, Russ. Chem. Bull. 53 (12) (2004) 2787–2792.
[75] A.C. Ferrari, J.C. Meyer, V. Scardaci, C. Casiraghi, M. Lazzeri, F. Mauri, S. Piscanec, D. Jiang, K.S. Novoselov, S. Roth, A.K. Geim, Raman spectrum of graphene and graphene layers, Phys. Rev. Lett. 97 (18) (2006) 187401.
[76] F. Torrisi, T. Hasan, W. Wu, Z. Sun, A. Lombardo, T.S. Kulmala, G.-W. Hsieh, S. Jung, F. Bonaccorso, P.J. Paul, D. Chu, A.C. Ferrari, Inkjet-printed graphene electronics, ACS Nano 6 (4) (2012) 2992–3006.
[77] A. Enotiadis, K. Angjeli, N. Baldino, I. Nicotera, D. Gournis, Graphene-based nafion nanocomposite membranes, enhanced proton transport and water retention by novel organo-functionalized graphene oxide nanosheets, Small 8 (21) (2012) 3338–3349.
[78] W. Choi, J. Choi, J. Bang, J.-H. Lee, Layer-by-layer assembly of graphene oxide nanosheets on polyamide membranes for durable reverse-osmosis applications, ACS Appl. Mater. Interfaces 5 (23) (2013) 12510–12519.
[79] F. Tuinstra, J.L. Koenig, Raman spectrum of graphite, J. Chem. Phys. 53 (3) (1970) 1126–1130.
[80] E.H. Martins Ferreira, M.V.O. Moutinho, F. Stavale, M.M. Lucchese, R.B. Capaz, C.A. Achete, A. Jorio, Evolution of the Raman spectra from single-, few-, and many-layer graphene with increasing disorder, Phys. Rev. B 82 (12) (2010) 125429.
[81] J.A. Leiro, M.H. Heinonen, T. Laiho, I.G. Batirev, Core-level Xps spectra of fullerene, highly oriented pyrolitic graphite, and glassy carbon, J. Electron. Spectrosc. Relat. Phenom. 128 (2–3) (2003) 205–213.
[82] G. Xing, J. Zhang, Y. Zhao, J. Tang, B. Zhang, X. Gao, H. Yuan, L. Qu, W. Cao, Z. Chai, K. Ibrahim, R. Su, Influences of structural properties on stability of fullerenols, J. Phys. Chem. B 108 (31) (2004) 11473–11479.
[83] Y.-B. Sun, C.-Y. Cao, S.-L. Yang, P.-P. Huang, C.-R. Wang, W.-G. Song, C60 fullerenol as an active and stable catalyst for the synthesis of cyclic carbonates from Co2 and epoxides, Chem. Commun. 50 (71) (2014) 10307–10310.
[84] K. Spyrou, M. Calvaresi, E.K. Diamanti, T. Tsoufis, D. Gournis, P. Rudolf, F. Zerbetto, Graphite oxide and aromatic amines, size matters, Adv. Funct. Mater. 25 (2) (2015) 263–269.
[85] K. Spyrou, L. Kang, E.K. Diamanti, R.Y. Gengler, D. Gournis, M. Prato, P. Rudolf, A novel route towards high quality fullerene-pillared graphene, Carbon 61 (2013) 313–320.
[86] Y. Song, S. Chang, S. Gradecak, J. Kong, Visibly-transparent organic solar cells on flexible substrates with all-graphene electrodes, Adv. Energy Mater. 6 (20) (2016) 1600847.
[87] T.R. Garrett, M. Bhakoo, Z. Zhang, Bacterial adhesion and biofilms on surfaces, Prog. Nat. Sci. 18 (9) (2008) 1049–1056.
[88] A. Krasowska, K. Sigler, How microorganisms use hydrophobicity and what does this mean for human needs?, Frontiers Cell Infect. Microbiol. 4 (112) (2014).
[89] K.-H. Chu, R. Xiao, E.N. Wang, Uni-directional liquid spreading on asymmetric nanostructured surfaces, Nat. Mater. 9 (2010) 413.
[90] E.S. Kooij, H.P. Jansen, O. Bliznyuk, B. Poelsema, H.J.W. Zandvliet, Directional wetting on chemically patterned substrates, Colloids Surf. A. Physicochem. Eng. Aspects 413 (2012) 328–333.